ACCEPTED MANUSCRIPT
Published in *COMPUTERS & STRUCTURES* (Volume 191, 15 October 2017, Pages 153-164)

(https://doi.org/10.1016/j.compstruc.2017.06.013)

A Computational Method for Automated Detection of Engineering Structures with Cyclic Symmetries

Yao Chen[1, 2*] Pooya Sareh[3] Jian Feng[1] Qiuzhi Sun[2]

[1] *National Prestress Engineering Research Center, and Key Laboratory of Concrete and Prestressed Concrete Structures of Ministry of Education, Southeast University, Nanjing 210096, China*

[2] *Jiangsu Key Laboratory of Engineering Mechanics, Southeast University, Nanjing 210096, China*

[3] *Department of Aeronautics, Faculty of Engineering, Imperial College of London, South Kensington Campus, London SW7 2AZ, United Kingdom*

Abstract: In general, for a complex engineering structure with a large number of nodes or members, the inherent symmetry is not easily recognizable. Even though someone succeeds in recognizing certain symmetry properties of the structure, these might be partial ones, and the others will be possibly unnoticed. To overcome this difficulty and enable the integration of computational analysis and symmetry methods, we propose an automated detection method for engineering structures with cyclic symmetries. Only the nodes and the connectivity patterns of the members are needed for implementing this algorithm. Using group theory, we first describe different cyclic groups of symmetries and their symmetry operations. In order to establish a group-theoretic algorithm for automated symmetry detection, several theorems and corollaries are presented. Then, on the basis of matrix representations of symmetry operations, the equivalence of the nodes and members of a structure is evaluated. Hence, the inherent symmetry operations of the structure are identified one by one. Illustrative examples show that the proposed automated symmetry detection method is robust and applicable to both 2D and 3D structures. Highly symmetric structures are recognized accurately and effectively. In addition, asymmetric structures and 2D structures can be recognized in a very small number of iterations.

Keywords: symmetry detection; cyclic group; group-theoretic algorithm; cable-strut; dome structure

* To whom correspondence should be addressed
E-mail: chenyao@seu.edu.cn

1. Introduction

In general, symmetry is scientifically significant because of its extremely rich and inspiring mathematics, as well as artistically attractive as a result of its remarkable aesthetic appeal. It occurs naturally in the world around us, and is of great importance in engineering analysis and design [1-4]. Utilizing symmetry can not only greatly simplify the analysis and reduce computational effort [5,6], but can also gain meaningful insights [7-10]. In fact, symmetry analysis is a powerful generative tool, which can be generalized for solving many engineering problems involving symmetry. For instance, to design innovative structures, a framework for deriving symmetric variations of the crease pattern of a given origami structure is presented [11]. The implementation of this framework leads to the design of an extensive family of folding structures which are either from the same symmetry group of the original structure [12] or are from one of its subgroups [10,13].

There are important and increasing real-world applications for this kind of analysis, given the tendency of architects and structural engineers to incorporate symmetry as well as subtle symmetry-breaking in their designs and analyses. Kaveh and Dadfar [2] have developed a symmetry method for calculating the buckling loads of symmetric 2D frame structures. Zingoni [14] has successfully utilized group theory for vibration problems in structural mechanics and obtained some effective insights and qualitative benefits. Chen and Feng [5,7] successfully applied symmetry analysis into Moore-Penrose inverse and integral prestress modes of cable-strut structures. Using symmetry-adapted compatibility matrices, Guest and Fowler [9] identified finite mechanisms in statically and kinematically indeterminate structures. Admittedly, to implement a symmetry analysis (e.g., the group-theoretic analysis), symmetry of a structure needs to be given or determined in advance [8,15]. Therefore, accurate symmetry detection is critical for effective and integrated symmetry analysis.

Symmetry detection is one of the fundamental ways to explore and understand the physical world around us, and thus has attracted interest from artists and scientists over centuries [16,17]. It can play an important role in

object recognition [18], image analysis [19], and classifications in computer vision [20,21]. Unfortunately, symmetry detection is traditionally performed manually, which is often tricky and time-consuming. In general, the symmetry of a complex structure with many nodes or members is not easily recognizable. Even though someone succeeds in recognizing certain symmetry properties of the structure, these might be partial ones, and the others will be possibly unnoticed [22]. To overcome this difficulty and enable an integrated symmetry analysis without human intervention, some automated symmetry detection algorithms have been presented [23]. Highnam [24] concerned a 2D point set, and simplified the original symmetry problems into a 1D pattern matching. He presented an algorithm capable of locating the symmetry axis for a reflection operation. Recently, Jiang et al. [16] have proposed a Fourier-theoretic method for determining the symmetry group G of an object. Using the Fourier transformations, a marginal-based search strategy has been proposed for detecting the symmetry group G. Nevertheless, the geometric similarity matrix which describes symmetry properties or their combinations need to be given beforehand. With the increasing demand for computer-aided design, Tate and Jared [25] proposed a computational method to identify the symmetry of regular geometries. In their method, the area of closed loops and the central point are calculated. Then, the symmetry is evaluated by pattern matching of the closed loops among various surfaces. However, this algorithm is highly time-consuming because of heavy computations on curved surfaces. Lee and Liu [26] extended the concept of two-fold reflection symmetry to curved glide-reflection symmetry in 2D. They successfully applied the curved glide-reflection axis detection for curved reflection surface detection in 3D.

Arguably, symmetry types remain to be specified in advance for the above-mentioned methods. In addition, they have not been closely integrated with group theory, which has a distinct advantage in analyzing symmetric systems. To avoid the manual specification of symmetry types, Zingoni [22] utilized symmetry operations and proposed an algorithm which can search for symmetry systematically. All existing rotation axes, whether

belonging to cyclic, dihedral, cubic or other symmetry groups, could be picked up by the three-dimensional search. The search for rotation axes has been made by sweeping over the entire spherical surface centered about the center of symmetry of the system, testing every possible position of the rotation axis. This search algorithm is very general, and shows good performance for the symmetric structures randomly dispersed in space. A key improvement for this algorithm is that it is intended for completely arbitrary system, and it does not assume any prior symmetry. Meanwhile, Zingoni [22] pointed out that the computation efficiency of the reported algorithm should be further enhanced. Many iterations will be needed to identify all symmetry operations for a constellation of a large number of points randomly distributed in three-dimensional space [22]. Suresh and Sirpotdar [23] made the full use of the basic concepts of group theory, and proposed a symmetry detection method for computer-aided design. The method is one of the very few methods which try to automate and integrate symmetry analysis, and provides an alternative way for symmetry detection.

On the other hand, computational effort of a low-order symmetric structure is approximately the same as that of a high-order one. In fact, for a low-order symmetric structure, some unnecessary computations can be avoided, which improves the computational efficiency significantly. Moreover, since many engineering structures are subjected to the gravity and have at most one feasible rotation axis, they generally belong to cyclic symmetry groups. Then, the symmetry search field for detecting these structures can be effectively reduced. Here, we will tackle a scenario where the structure is known at the outset to possess cyclic symmetry, which allows simplifications over the more general approaches reported in [22] and [23]. We will propose an efficient and automated symmetry detection method for 2D and 3D engineering structures with cyclic symmetries. Only the nodal coordinates and the connectivity patterns of the members are needed for implementing this algorithm. Note that this automated symmetry detection method will be preferred for symmetry analysis. Furthermore, in combination with frequently used methods of structural design, this method can provide us with a powerful tool

for the design of symmetric structures. For instance, this method can be generalized to design novel mechanisms [6,27], or to develop innovative forms of tensegrity structures [28-30]. Moreover, a future improvement of this research can link it to computer vision, where a vision-based algorithm can detect the symmetry properties of the structure from one or more 3D images or 2D pictorial views [31-33].

The content of this work is as follows. Section 2 describes different groups of cyclic symmetry and their symmetry operations. Section 3 proposes the automated symmetry detection method, in which the equivalence of the geometric configuration of a structure is evaluated. Then, in Section 4, a large variety of numerical examples are presented to verify the effectiveness of the proposed method. Finally, conclusions are given in Section 5.

2. Symmetry Operations and Symmetry Groups

2.1. Symmetry operations

A 2D or 3D structure is said to be symmetric if its structural configuration remains invariant under certain independent linear transformations. These transformations are defined as symmetry operations [34]. For all finite engineering structures, symmetry operations are classified into five types:

(I) The identity, *E*. This symmetry operation describes that no actual transformation is applied to the structure, and thus the configuration remains unchanged. In fact, the identity *E* is possessed by all kinds of structures.

(II) The rotation operation, C_n^i. It denotes a counterclockwise (or clockwise) rotation by an angle $\alpha = 2\pi i/n$ about an axis. For the integer *n* we should have $n \geq 2$, and $i \in [1, n-1]$. The axis is also known as the *n*-fold rotation axis.

(III) The reflection operation with respect to a symmetry (mirror) plane, σ_i. Generally, σ_v denotes a reflection with respect to a vertical symmetry plane, which contains the principal axis. σ_h denotes a reflection with respect to a horizontal symmetry plane, which is perpendicular to the principal axis.

(IV) The improper rotation operation, S_{2n}^{2i-1}. It denotes a rotation by an angle $\alpha = (2i-1)\pi/n$ about a

rotation axis ($i \in [1, n]$), preceded with a reflection with respect to a symmetry plane perpendicular to the axis. This operation is also known as the rotation-reflection operation, and satisfies

$$S_{2n}^{2i-1} = \sigma_h \cdot C_{2n}^{2i-1} \tag{1}$$

(V) The inversion operation, S_2. It is an inversion through the center unshifted by all symmetry operations. Moreover, it is a special case of the improper rotation with n=1,

$$S_2^1 = \sigma_h \cdot C_2^1 \tag{2}$$

Figs. 1(a-d) respectively show different kinds of symmetry operations listed above (except the identity, E), where the members keep equivalent under these operations.

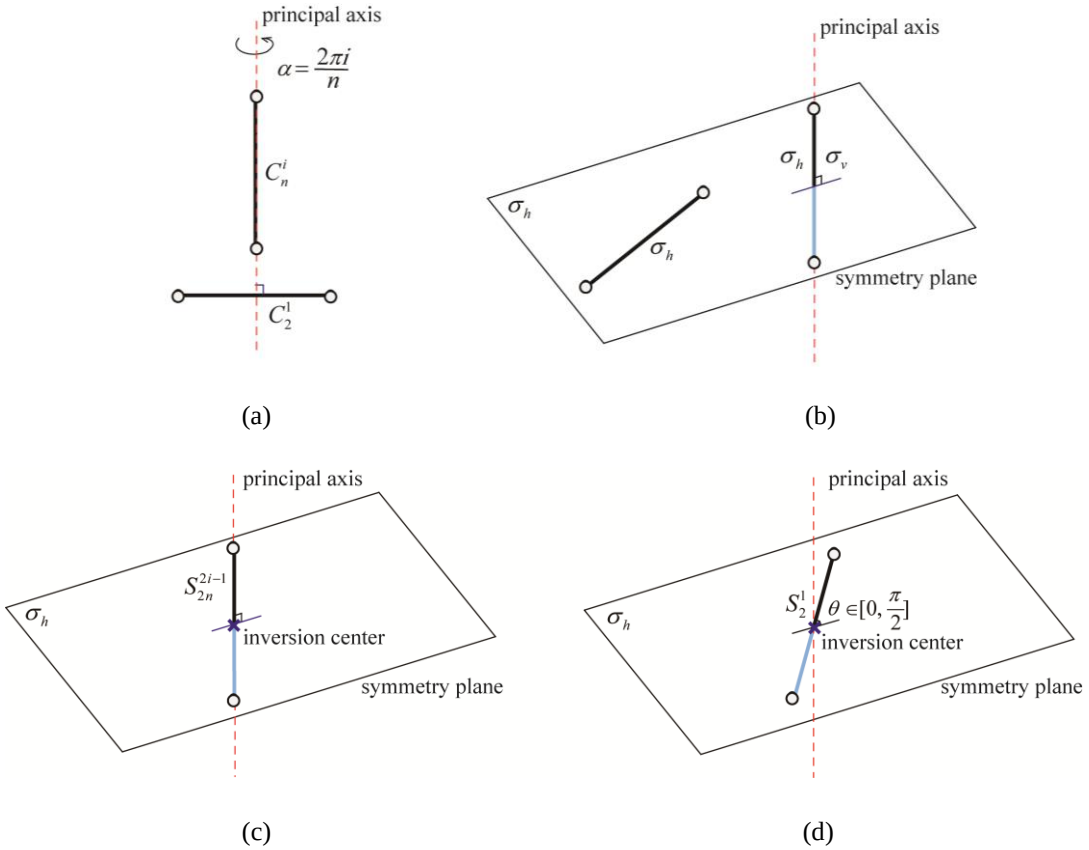

Figure 1 Different kinds of symmetry operations: (a) rotation C_n^i; (b) reflection σ_i; (c) improper rotation S_{2n}^{2i-1}; (d) inversion S_2^1

2.2. Matrix representations for different symmetry operations

Each symmetry operation which transforms a finite structure into itself must keep the center of the structure

unshifted. More importantly, this center coincides with the inversion center of symmetry. Without loss of generality, supposing that a certain symmetric structure is composed of m_0 nodes and b members, the initial coordinates of a node $j \in [1,\ m_0]$ is $(x_j,\ y_j,\ z_j)$ in the Cartesian coordinate system XYZ. We take z_j=0 for 2D structures. Then, the center of the structure $O(x_0,\ y_0,\ z_0)$ is computed by

$$x_0 = \frac{1}{m_0}\sum_{j=1}^{m_0} x_j\ ,\quad y_0 = \frac{1}{m_0}\sum_{j=1}^{m_0} y_j\ ,\quad z_0 = \frac{1}{m_0}\sum_{j=1}^{m_0} z_j \tag{3}$$

where the geometry center O is assumed to coincide with the center-of-mass of the structure. To locate the center O at the origin of the symmetry coordinate system, the initial coordinate system is translated. In the new coordinate system $\overline{XYZ}$, the nodal vector $\boldsymbol{X}_j$ for each node $j \in [1,\ m_0]$ is expressed by

$$\boldsymbol{X}_j = [\overline{x_j},\ \overline{y_j},\ \overline{z_j}]^{\mathrm{T}} = [x_j - x_0,\ y_j - y_0,\ z_j - z_0]^{\mathrm{T}} \tag{4}$$

Mathematically speaking, each symmetry operation is a linear transformation on the nodal vectors of the structure. As the coordinate system has been attached to the structure, we can describe the matrix representations for all the symmetry operations. Subjected to the identity operation E, the new vector of one node $j \in [1,\ m_0]$ is written as

$$\boldsymbol{X}_{j,E} = \boldsymbol{R}_E \cdot \boldsymbol{X}_j = \begin{bmatrix} 1 & 0 & 0 \\ 0 & 1 & 0 \\ 0 & 0 & 1 \end{bmatrix} \cdot \begin{bmatrix} \overline{x_j} \\ \overline{y_j} \\ \overline{z_j} \end{bmatrix},\quad \forall j \in [1,\ m_0] \tag{5}$$

where $\boldsymbol{X}_{j,E} = [x_{j,E},\ y_{j,E},\ z_{j,E}]^{\mathrm{T}}$ is the new nodal vector, and the 3×3 identity matrix $\boldsymbol{R}_E$ is the corresponding transformation matrix. Eq. (5) shows that each node remains unshifted under the identity operation E.

Under a rotation operation C_n^i about the Z-axis, the new vector of node $j \in [1,\ m_0]$ is written as

$$\boldsymbol{X}_{j,C_n^i} = \boldsymbol{R}_{C_n^i} \cdot \boldsymbol{X}_j = \begin{bmatrix} \cos(2\pi i/n) & -\sin(2\pi i/n) & 0 \\ \sin(2\pi i/n) & \cos(2\pi i/n) & 0 \\ 0 & 0 & 1 \end{bmatrix} \cdot \begin{bmatrix} \overline{x_j} \\ \overline{y_j} \\ \overline{z_j} \end{bmatrix},\quad \forall j \in [1,\ m_0]\ ,\quad i \in [1, n-1] \tag{6}$$

where $\boldsymbol{X}_{j,C_n^i} = [x_{j,C_n^i},\ y_{j,C_n^i},\ z_{j,C_n^i}]^{\mathrm{T}}$ is the new nodal vector, and the 3×3 matrix $\boldsymbol{R}_{C_n^i}$ is the transformation

matrix for the rotation C_n^i. In addition, when $i = n$ in Eq. (6),

$$\boldsymbol{R}_{C_n^n} = \boldsymbol{R}_E = \begin{bmatrix} 1 & 0 & 0 \\ 0 & 1 & 0 \\ 0 & 0 & 1 \end{bmatrix} \tag{7}$$

Thus, the rotation C_n^n is equivalent to the identity operation *E*. On the other hand, if a structure remains invariant under a reflection operation σ_v on the vertical symmetry plane, it satisfies

$$\boldsymbol{X}_{j,\sigma_v} = \boldsymbol{R}_{\sigma_v} \cdot \boldsymbol{X}_j = \begin{bmatrix} \cos(2\alpha_r) & \sin(2\alpha_r) & 0 \\ \sin(2\alpha_r) & -\cos(2\alpha_r) & 0 \\ 0 & 0 & 1 \end{bmatrix} \cdot \begin{bmatrix} \overline{x_j} \\ \overline{y_j} \\ \overline{z_j} \end{bmatrix}, \quad \forall j \in [1, m_0], \quad \alpha_r \in [0, \pi) \tag{8}$$

where $\boldsymbol{X}_{j,\sigma_v} = [x_{j,\sigma_v}, y_{j,\sigma_v}, z_{j,\sigma_v}]^{\mathrm{T}}$ is the shifted nodal vector, and the 3×3 matrix $\boldsymbol{R}_{\sigma_v}$ is the transformation matrix for the rotation σ_v. The vertical symmetry plane contains the *Z*-axis, and it is perpendicular to the *XY* plane. In Eq. (8), α_r denotes the angle between the *XZ* plane and the symmetry plane. Similarly, if a structure keeps equivalent under a reflection operation σ_h with respect to the horizontal symmetry plane, it satisfies

$$\boldsymbol{X}_{j,\sigma_h} = \boldsymbol{R}_{\sigma_h} \cdot \boldsymbol{X}_j = \begin{bmatrix} 1 & 0 & 0 \\ 0 & 1 & 0 \\ 0 & 0 & -1 \end{bmatrix} \cdot \begin{bmatrix} \overline{x_j} \\ \overline{y_j} \\ \overline{z_j} \end{bmatrix}, \forall j \in [1, m_0] \tag{9}$$

where $\boldsymbol{X}_{j,\sigma_h} = [x_{j,\sigma_h}, y_{j,\sigma_h}, z_{j,\sigma_h}]^{\mathrm{T}}$ is the nodal vector, and the matrix $\boldsymbol{R}_{\sigma_h}$ is the corresponding transformation matrix.

Under an improper rotation operation S_{2n}^{2i-1} about the *Z*-axis, the new vector of node $j \in [1,\ m_0]$ is written as

$$\boldsymbol{X}_{j,S_{2n}^{2i-1}} = \boldsymbol{R}_{S_{2n}^{2i-1}} \cdot \boldsymbol{X}_j = \begin{bmatrix} \cos((2i-1)\pi/n) & -\sin((2i-1)\pi/n) & 0 \\ \sin((2i-1)\pi/n) & \cos((2i-1)\pi/n) & 0 \\ 0 & 0 & -1 \end{bmatrix} \cdot \begin{bmatrix} \overline{x_j} \\ \overline{y_j} \\ \overline{z_j} \end{bmatrix} \forall j \in [1, m_0], \quad i \in [1, n] \tag{10}$$

where $\boldsymbol{X}_{j,S_{2n}^{2i-1}} = [x_{j,S_{2n}^{2i-1}}, y_{j,S_{2n}^{2i-1}}, z_{j,S_{2n}^{2i-1}}]^{\mathrm{T}}$ is the shifted nodal vector by the operation S_{2n}^{2i-1}, and the matrix $\boldsymbol{R}_{S_{2n}^{2i-1}}$ is the 3×3 transformation matrix. As the inversion operation S_2^1 is a special case of the improper rotation operations, its matrix representation can be computed from Eq. (10), with *n*=*i*=1. Thus, we have

$$\boldsymbol{X}_{j,S_2^1} = \boldsymbol{R}_{S_2^1} \cdot \boldsymbol{X}_j = \begin{bmatrix} -1 & 0 & 0 \\ 0 & -1 & 0 \\ 0 & 0 & -1 \end{bmatrix} \cdot \begin{bmatrix} \overline{x_j} \\ \overline{y_j} \\ \overline{z_j} \end{bmatrix}, \quad \forall j \in [1, m_0] \tag{11}$$

where $\boldsymbol{X}_{j,S_2^1} = [x_{j,S_2^1}, y_{j,S_2^1}, z_{j,S_2^1}]^{\mathrm{T}}$ is the shifted nodal vector by the inversion S_2^1, and the matrix $\boldsymbol{R}_{S_2^1}$ is the transformation matrix. It is important to mention that the matrix representations in Eqs. (6)-(11) are expressed in terms of the Cartesian coordinate system, whereas the *Z*-axis is the principal axis of symmetry. Indeed, they are also applicable to other coordinate systems, with a series of linear transformations through the new coordinate system.

2.3. Cyclic symmetry groups

A group $G=\{g_1, g_2, \cdots, g_i \cdots\}$ is called a *symmetry group*, on condition that all the elements g_i of G are symmetry operations. Furthermore, the number of symmetry operations included in a symmetry group determines the order of the group, $|G|$. A symmetry group is known as point symmetry group, when at least one point of the system remains fixed under the action of all the symmetry operations.

Point symmetry groups can be classified into cyclic groups, dihedral groups and cubic groups [35]. Dihedral and cubic groups possess many different rotation axes [29], e.g., the two-fold, three-fold or five-fold rotation axis [30]. Here, we concern the cyclic groups, because many symmetric structures for engineering applications subject to the gravity and have no more than a single rotation axis [36,37]. All cyclic groups and their symmetry operations are summarized in Table 1, where the positive integer $n \geq 2$ [38].

Note that the notations in Table 1 such as C_n and C_{nh} refer to the Schoenflies notations of (point) cyclic symmetry groups [38]. A low-order symmetry group has no rotation operation, and its order is at most 2. Notably, a symmetric structure that belongs to the lowest-order group C_1 refers to an asymmetric structure. On the other hand, a regular symmetry group has a principal axis for the *n*-fold rotation. Specifically, proper cyclic group C_n contains only *n* rotations about the principal axis; proper cyclic group C_{nv} is C_n with the addition of *n*

reflections along the vertical symmetric planes; proper cyclic group C_{nh} is C_n with the addition of a reflection along the horizontal symmetry plane; and improper cyclic group S_{2n} is C_n with the addition of n improper rotations along the principal axis.

Table 1 Cyclic symmetry groups and their symmetry operations

Low-order symmetry			Regular symmetry		
Group	Order	Symmetry operations	Group	Order	Symmetry operations
C_1	1	E	C_n	n	$E,\ C_n^i\ (i=1,\cdots,n-1)$
$C_s=C_h$	2	E,σ_h	C_{nv}	$2n$	$E,\ C_n^i(i=1,\cdots,n-1),\ n\sigma_v$
$S_2=C_i$	2	E,S_2^1	C_{nh}	n+1	$E,\ C_n^i(i=1,\cdots,n-1),\ \sigma_h$
			S_{2n}	$2n$	$E,\ C_n^i(i=1,\cdots,n-1),\ S_{2n}^{2i-1}(i=1,...,n)$

Despite the huge diversity of structural configurations in engineering, the associated symmetry operations are finite. According to Table 1, once all the symmetry operations for a given structure are identified, the highest-order symmetry group of the structure can be determined.

3. Automated Symmetry Detection Method

3.1. Theorems and corollaries

On the basis of symmetry operations and their matrix representations, the following theorems and corollaries are presented, which are important for establishing the automated symmetry detection method.

Theorem 1. If a symmetric structure remains invariant under a rotation C_n^i (or S_{2n}^{2i-1}) about an axis, then it must remain invariant under the operation $C_{n'}^{i'}$ (or $S_{2n'}^{2i'-1}$) about the same axis. The positive integer n' is a divisor of n, where $n'\geq 2$, $1\leq i'\leq n'$ and $1\leq i\leq n$.

Proof. It can be obtained from Eqs. (6) and (10) that the transformation matrices $\boldsymbol{R}_{C_{n'}^{i'}}$ and $\boldsymbol{R}_{S_{2n'}^{2i'-1}}$ are

$$\boldsymbol{R}_{C_{n'}^{i'}}=\begin{bmatrix}\cos(2\pi i'/n') & -\sin(2\pi i'/n') & 0\\ \sin(2\pi i'/n') & \cos(2\pi i'/n') & 0\\ 0 & 0 & 1\end{bmatrix},\quad \boldsymbol{R}_{S_{2n'}^{2i'-1}}=\begin{bmatrix}\cos((2i'-1)\pi/n') & -\sin((2i'-1)\pi/n') & 0\\ \sin((2i'-1)\pi/n') & \cos((2i'-1)\pi/n') & 0\\ 0 & 0 & -1\end{bmatrix},\quad i'\in[1,n'] \tag{12}$$

Note that $\{2\pi i'/n' \,|\, 1\le i'\le n'\}\subset\{2\pi i/n \,|\, 1\le i\le n\}$, and $\{(2i'-1)\pi/n' \,|\, 1\le i'\le n'\}\subset\{(2i-1)\pi/n \,|\, 1\le i\le n\}$, because n' is a divisor of n. For example, $n'=3$ is a divisor of $n=6$, and we have $\{2\pi/3,\ 4\pi/3,\ 2\pi\}\subset\{\pi/3,\ 2\pi/3,\ \pi,\ 4\pi/3,\ 5\pi/3,\ 2\pi\}$.

Then the transformation matrices $\boldsymbol{R}_{C_{n'}^{i'}}$ and $\boldsymbol{R}_{S_{2n'}^{2i'-1}}$ are, respectively, included in the matrices $\boldsymbol{R}_{C_n^i}$ and $\boldsymbol{R}_{S_{2n}^{2i-1}}$. Therefore, we have proved that if a structure retains a rotation C_n^i (or S_{2n}^{2i-1}) about an axis, then it must retain the operation $C_{n'}^{i'}$ (or $S_{2n'}^{2i'-1}$) about the same axis.

Corollary. If a structure remains invariant under two rotations $C_{n_1}^1$ and $C_{n_2}^1$ (or $S_{2n_1}^1$, $S_{2n_2}^1$) about an axis, then it must remain invariant under the operation C_n^1 (or S_{2n}^1) about the same axis. The positive integer n is the least common multiple of n_1 and n_2.

Proof. Supposing that node j is transformed from node j_1 under rotation $C_{n_1}^1$, and node j_1 is transformed from node j_2 under rotation $C_{n_2}^1$, the matrix representation for the nodes is expressed as

$$\begin{bmatrix}\overline{x_j}\\ \overline{y_j}\\ \overline{z_j}\end{bmatrix}=\boldsymbol{R}_{C_{n_1}^1}\cdot\boldsymbol{X}_{j_1}=\boldsymbol{R}_{C_{n_1}^1}\cdot\boldsymbol{R}_{C_{n_2}^1}\cdot\boldsymbol{X}_{j_2}=\begin{bmatrix}\cos(2\pi(n_1+n_2)/n_1n_2) & -\sin(2\pi(n_1+n_2)/n_1n_2) & 0\\ \sin(2\pi(n_1+n_2)/n_1n_2) & \cos(2\pi(n_1+n_2)/n_1n_2) & 0\\ 0 & 0 & 1\end{bmatrix}\cdot\begin{bmatrix}\overline{x_{j_2}}\\ \overline{y_{j_2}}\\ \overline{z_{j_2}}\end{bmatrix}, \tag{13}$$

As the integer n is the least common multiple of n_1 and n_2, we can rewrite Eq. (13) as

$$\begin{bmatrix}\overline{x_j}\\ \overline{y_j}\\ \overline{z_j}\end{bmatrix}=\boldsymbol{R}_{C_n^i}\cdot\boldsymbol{X}_{j_2}=\begin{bmatrix}\cos(2\pi i/n) & -\sin(2\pi i/n) & 0\\ \sin(2\pi i/n) & \cos(2\pi i/n) & 0\\ 0 & 0 & 1\end{bmatrix}\cdot\begin{bmatrix}\overline{x_{j_2}}\\ \overline{y_{j_2}}\\ \overline{z_{j_2}}\end{bmatrix}\text{ and }\ 1\le i\le n \tag{14}$$

Hence, this corollary is proved by combining Eq. (14) with Eq. (6).

Theorem 2. If a structure is symmetric, then the distances from the center of the structure to at least two nodes are identical.

Proof. For a symmetric structure, the principal axis or symmetry plane passes through the symmetry center of the structure. Under every symmetry operation, the nodes on the same orbit remain invariant. Thus, the distances from these nodes to the center of the structure are identical.

Corollary 1. If a structure remains invariant under a symmetry operation C_n^i or S_{2n}^{2i-1} about an axis ($1\le i\le n-1$, where i and n are relatively prime), then the distances from the center of the structure to at least n

nodes are identical.

Proof. Eqs. (6) and (10) show that at least *n* nodes are on the same orbit and remain invariant under the operation C_n^i or S_{2n}^{2i-1}.

Corollary 2. If a structure remains invariant under a rotation C_n^i ($1 \le i \le n-1$, where *i* and *n* are relatively prime), and a reflection operation σ_v on a vertical symmetry plane, then the structure retains at least *n* reflection operations along *n* different vertical symmetry planes.

Proof. Supposing that node *j* is transformed from node j_1 under rotation C_n^i, and node j_1 is transformed from node j_2 under reflection σ_v, the matrix representation for the nodes is expressed as

$$\begin{bmatrix} \overline{x_j} \\ \overline{y_j} \\ \overline{z_j} \end{bmatrix} = \boldsymbol{R}_{C_n^i} \cdot \boldsymbol{R}_{\sigma_v} \cdot \boldsymbol{X}_{j_2} = \begin{bmatrix} \cos(2\alpha_r + 2\pi i/n) & \sin(2\alpha_r + 2\pi i/n) & 0 \\ \sin(2\alpha_r + 2\pi i/n) & -\cos(2\alpha_r + 2\pi i/n) & 0 \\ 0 & 0 & 1 \end{bmatrix} \cdot \begin{bmatrix} \overline{x_{j_2}} \\ \overline{y_{j_2}} \\ \overline{z_{j_2}} \end{bmatrix}, \quad \forall j \in [1, m_0], \quad i \in [1, n-1] \tag{15}$$

Thus, it can be concluded from Eq. (8) that the structure has *n* reflection operations, where $\alpha_r + \pi i/n$ in Eq. (15) determines the angle between the *XZ* plane and the corresponding symmetry plane.

3.2. Further improvements on the computation efficiency

The distance from the center of the structure to a node *j* is defined as

$$r_j = \sqrt{\overline{x_j}^2 + \overline{y_j}^2 + \overline{z_j}^2}, \quad \forall j \in [1, m_0] \tag{16}$$

and the maximum number of nodes with identical r_j is denoted by n_r, whereas the allowable tolerance ε for the numerical computations is taken as

$$\varepsilon = \max(10^{-3}, 10^{-4} r_{\max}) \tag{17}$$

where $r_{\max}$ is the maximum of r_j. Then, according to Theorem 2 and its corollaries, we can evaluate the value of *n* from the interval

$$2 \le n \le n_r \tag{18}$$

Thereafter, the computational effort for determining the *n*-fold axis and the rotation angle α will be significantly reduced. More importantly, a structure is guaranteed to be asymmetric when $n_r = 1$; that is, each node has a different distance r_j to the center of the structure. Using this criterion, asymmetric structures can be

efficiently detected.

For generality, the authors also concern the case that a 3D cyclically symmetric structure is randomly oriented in space. Then, the principal axis should be first identified. Since a general member k_1 moves on to another member k_2 with an identical length $l_{k_1} = l_{k_2}$ under a rotation around the principal axis, the principal axis $\boldsymbol{n}_z$ can be effectively determined by

$$\boldsymbol{n}_z \subset \left\{ \boldsymbol{n}_{k_1} \times \boldsymbol{n}_{k_2} \,\middle|\, \forall k_1, k_2 \in [1, b] \text{ and } l_{k_1} = l_{k_2} \right\} \tag{19}$$

where $\boldsymbol{n}_{k_1}$ and $\boldsymbol{n}_{k_2}$ are the unit vectors along the members k_1 and k_2, and $\boldsymbol{n}_{k_1} \times \boldsymbol{n}_{k_2}$ denotes the cross product. Hence, one candidate axis of the potential axes is chosen as the principal axis, which is obtained the most times from Eq. (19). It should be noted that the horizontal symmetry plane is perpendicular to the principal axis, which lies in each vertical symmetry plane. Based on the definition of a reflection on a symmetry plane, the normal $\boldsymbol{n}_{\sigma_v}$ of a vertical symmetry plane must be parallel to one of the vectors which connect two nodes with identical r_j. That is

$$\boldsymbol{n}_{\sigma_v} \subset \left\{ \frac{\boldsymbol{X}_{j_1} - \boldsymbol{X}_{j_2}}{\left\| \boldsymbol{X}_{j_1} - \boldsymbol{X}_{j_2} \right\|_2} \,\middle|\, \forall j_1, j_2 \in [1, m_0] \text{ and } r_{j_1} = r_{j_1} \right\}, \text{ and } \boldsymbol{n}_{\sigma_v} \cdot \boldsymbol{n}_z = 0 \tag{20}$$

where $\left\| \boldsymbol{X}_{j_1} - \boldsymbol{X}_{j_2} \right\|_2$ denotes the distance between the nodes j_1 and j_2. At the beginning of the symmetry detection, it is assumed that $\boldsymbol{n}_{\sigma_v} = [0 \;\; 1 \;\; 0]^{\mathrm{T}}$, and $\boldsymbol{n}_z = [0 \;\; 0 \;\; 1]^{\mathrm{T}}$. When a given structure retains no reflection (i.e., no solution exists for Eq. (20)), the vector $\boldsymbol{n}_{\sigma_v}$ is still taken as $\boldsymbol{n}_{\sigma_v} = [0 \;\; 1 \;\; 0]^{\mathrm{T}}$.

To detect cyclic symmetry of a structure along desired orientations, the coordinates of a general symmetric structure shall be transformed in terms of a modified coordinate system

$$\boldsymbol{X}_j = \boldsymbol{R}_{XYZ} \cdot [x_j - x_0, y_j - y_0, z_j - z_0]^{\mathrm{T}}, \quad \forall j \in [1, m_0] \tag{21}$$

In this modified right-handed system, the principal axis $\boldsymbol{n}_z$ is taken as the *Z*-axis, and $\boldsymbol{n}_{\sigma_v}$ is taken as the *Y*-axis. The 3×3 direction cosine matrix $\boldsymbol{R}_{XYZ}$ in Eq. (21) is written as

$$\boldsymbol{R}_{XYZ}=\begin{bmatrix}\cos(\boldsymbol{n}_{\sigma_v}\times\boldsymbol{n}_z,X) & \cos(\boldsymbol{n}_{\sigma_v}\times\boldsymbol{n}_z,Y) & \cos(\boldsymbol{n}_{\sigma_v}\times\boldsymbol{n}_z,Z)\\ \cos(\boldsymbol{n}_{\sigma_v},X) & \cos(\boldsymbol{n}_{\sigma_v},Y) & \cos(\boldsymbol{n}_{\sigma_v},Z)\\ \cos(\boldsymbol{n}_z,X) & \cos(\boldsymbol{n}_z,Y) & \cos(\boldsymbol{n}_z,Z)\end{bmatrix} \tag{22}$$

where $\boldsymbol{n}_{\sigma_v}\times\boldsymbol{n}_z$ denotes the new *X*-axis, and $\cos(\boldsymbol{n}_{\sigma_v},X)$ in the matrix $\boldsymbol{R}_{XYZ}$ denotes the direction cosine of the new *Y*-axis (the vector $\boldsymbol{n}_{\sigma_v}$) with respect to the original *X*-axis. Similarly, the other entries in Eq. (22) can be obtained.

On the other hand, computation efficiency of the symmetry detection method can be further improved by considering the symmetry of distinguishing characteristics or mechanical properties. For example, the symmetry of the material properties, the symmetry of the cross-sectional areas of members, and that of boundary conditions are G_e, G_a, and G_b, respectively. Then, the actual symmetry group *G* for the given engineering structure is

$$G=\text{lowest-order group of }(G_1,G_e,G_a,G_b) \tag{23}$$

where G_1 is the symmetry group of the nodes and connectivity patterns. However, it should be noted that the symmetry of external loads does not alter the symmetry group G of the given structure. Even if the external loads have lower-order symmetry or asymmetry, they can be decomposed into a series of vectors in the symmetry-adapted coordinate system and solved independently [10,39,40].

3.3. Group-theoretic algorithm

Based on the characteristics of different symmetry groups in Table 1 and the above-mentioned theorems and corollaries, Fig. 2 gives the flowchart for detecting the cyclic symmetry group of a given engineering structure. The kernel of this algorithm contains seven steps.

Step 1. The structural configuration (e.g., nodal coordinates and connectivity patterns of members) is provided as initial input data. Subsequently, modify the nodal coordinates using Eqs. (3)-(4), to locate the symmetry center at the origin of a new coordinate system.

Step 2. Compute the distance r_j from the center of the structure to each node $j\in[1,m_0]$ by Eq. (16), and

determine whether the value of n_r in Eq. (18) is smaller than 2. If $n_r < 2$, finish this algorithm; and thus the structure is asymmetric and belongs to the lowest-order C_1 group. Otherwise, modify the symmetry coordinate system using Eqs. (19)-(22), and go to Step 3 for further symmetry detection.

Step 3. For the value of *n* decreased from n_r to 2, iteratively evaluate whether the structure contains a C_n^1 rotation along the principal axis, where the transformation matrix is based on the matrix representation for the rotation operation in Eq. (6) with $i = 1$. If yes, obtain the exact value of *n*, denote $f_c = 1$, and then terminate the iteration. Otherwise, $f_c = 0$, $n = n - 1$, and continue for the iteration while $n > 2$. Go to Step 4.

Step 4. Evaluate whether the structure contains a vertical symmetry plane, where the transformation matrix is based on the matrix representation in Eq. (8). If yes, $f_{\sigma_v} = 1$; otherwise, $f_{\sigma_v} = 0$. Then,

a) If $f_c = f_{\sigma_v} = 1$, finish this algorithm; and thus the structure is C_{nv} symmetric ($n \geq 2$).

b) If $f_c = 1$, $f_{\sigma_v} = 0$, and the structure is 2D, then the structure is C_n symmetric ($n \geq 2$). Finish this algorithm.

c) Otherwise, go to Step 5.

Step 5. Evaluate whether the structure contains a horizontal symmetry plane, where the transformation matrix is based on the matrix representation in Eq. (9). If yes, $f_{\sigma_h} = 1$; otherwise, $f_{\sigma_h} = 0$. Then,

a) If $f_c = 0$ and $f_{\sigma_v} + f_{\sigma_h} > 0$, finish this algorithm; and thus the structure is C_s (or C_h) symmetric.

b) If $f_c = 1$ and $f_{\sigma_h} = 1$, finish this algorithm; and thus the structure is C_{nh} symmetric.

c) If $f_c = f_{\sigma_v} = f_{\sigma_h} = 0$, go to Step 6.

d) Otherwise, go to Step 7.

Step 6. Evaluate whether the structure contains an inversion, where the transformation matrix is based on the matrix representation in Eq. (11). If yes, the structure is C_i symmetric; otherwise, the structure is asymmetric (i.e., C_1 group). The automated symmetry detection algorithm is finished.

Step 7. Evaluate whether the structure contains an improper rotation S_{2n}^1 along the principal axis, where the transformation matrix is based on the matrix representation in Eq. (10) and i=1. If yes, the structure is S_{2n} symmetric; otherwise, the structure is C_n symmetric. The algorithm is finished.

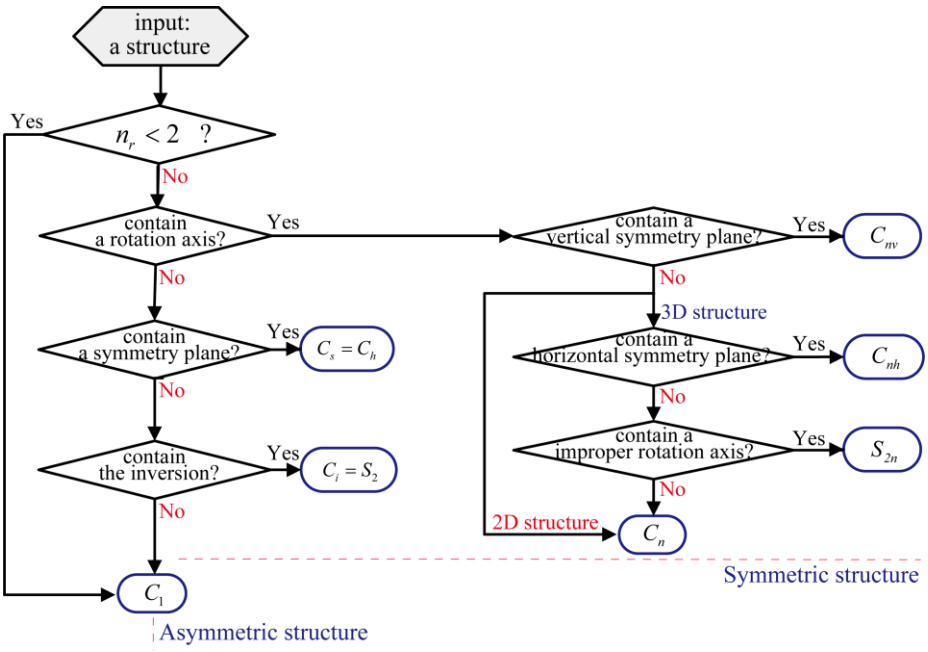

Figure 2 Flowchart for detecting the cyclic symmetry group of a given engineering structure

As can be seen in Fig. 2 and the above-mentioned algorithm, Steps 5 and 7 are not necessary for all 2D structures. This is because all the nodes and members of 2D structures locate on the same plane. Consequently, this proposed detection method allows much more efficient evaluations for 2D structures.

At each step of the automated symmetry detection algorithm, the key is to evaluate the equivalence of the geometric configuration of a given structure. To evaluate the equivalence of nodes, a set $\boldsymbol{N}$ which collects nodal vectors $\boldsymbol{X}_j$ is denoted by

$$\boldsymbol{N} = \left\{ \boldsymbol{X}_j \,\middle|\, j \in [1, m_0] \right\} \tag{24}$$

and $\boldsymbol{N}_S = \left\{ \boldsymbol{X}_{j,S} \,\middle|\, j \in [1, m_0] \right\}$ is the corresponding set that collects the new nodal vectors $\boldsymbol{X}_{j,S}$ under the operation S. These sets can be taken as equivalent if they satisfy

$$\boldsymbol{N} \approx \boldsymbol{N}_S \tag{25}$$

where $\approx$ indicates that the precision of nodal vectors is broadened, because of the accuracy of numerical computations, and potential surds and square roots involved in symmetry operations. Besides, another set $\boldsymbol{M}$ which collects the connectivity patterns of members is denoted by

$$\boldsymbol{M} = \left\{ \boldsymbol{K}_m \,\middle|\, m \in [1, b] \right\} \tag{26}$$

where the two-dimensional vector $\boldsymbol{K}_m = [i,\ j]$ describes that a general member $m \in [1, b]$ connects the nodes i and j, and $i<j$. On condition that the nodes remain invariant under the operation S, we need to further evaluate the equivalence of members, and build the corresponding set $\boldsymbol{M}_S$ for the members

$$\boldsymbol{M}_S = \left\{ \boldsymbol{K}_{m,S} \,\middle|\, m \in [1, b] \right\} \tag{27}$$

In Eq. (27), $\boldsymbol{K}_{m,S} = [i_S,\ j_S]$, where the node i is transformed from node i_S under the operation S, and the node j is transformed from node j_S. Then, under the operation S, the connectivity of members can be taken as equivalent if

$$\boldsymbol{M} \cup \boldsymbol{M}_S = \boldsymbol{M} \cap \boldsymbol{M}_S \tag{28}$$

which reveals that the involved operation is a symmetry operation and brings all the members into coincidence with themselves. In a word, we should search for the feasible solution to Eqs. (25) and (28) at each iteration step of Fig. 2.

4. Illustrative Examples for Symmetry Detection of Certain Structures with Cyclic Symmetries

A large number of symmetric structures are presented to evaluate the performance of the proposed symmetry detection method. In these examples, the symmetry center remains invariant, and the Z-axis is taken as the principal axis. All the examples are implemented in MATLAB on a PC with 3.1 GHz CPU and 4 GB RAM.

4.1. 2D symmetric structures

Figure 3 gives eleven examples of 2D symmetric structures. Based on their configurations and the automated

detection algorithm, the symmetry properties and the corresponding running time of the proposed approach for these structures are obtained and shown in Table 2.

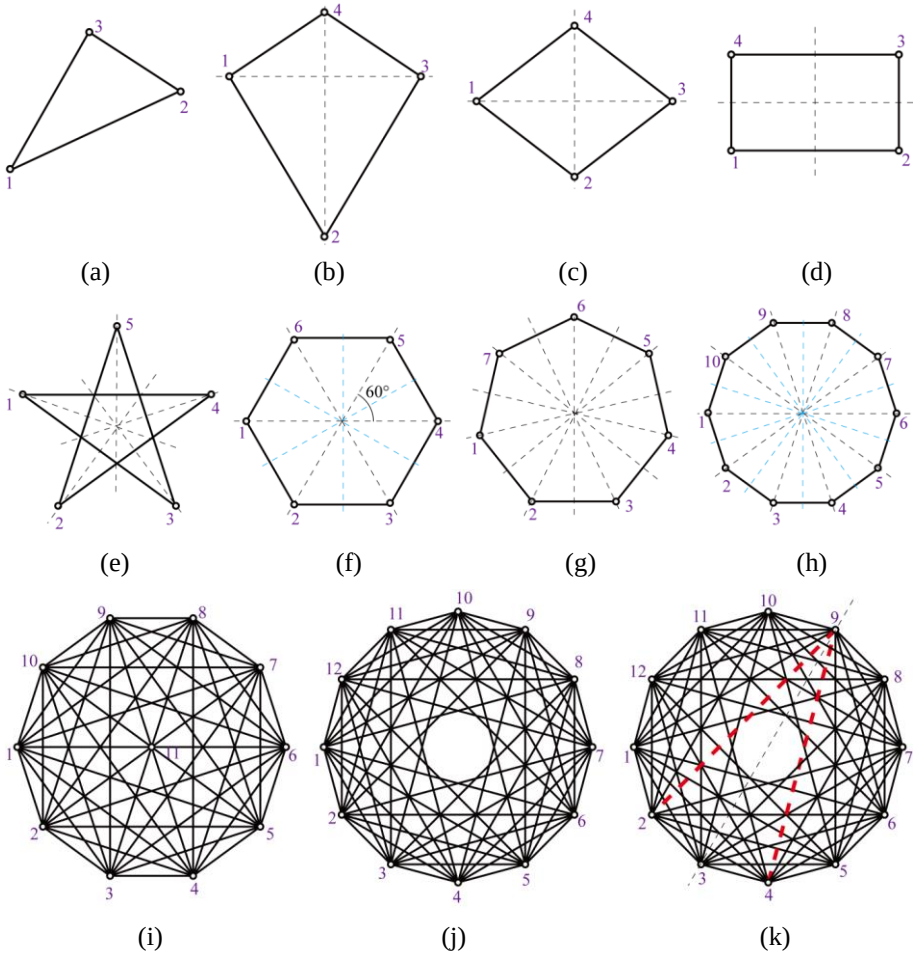

Figure 3 2D symmetric structures

Table 2 Running time and symmetry properties for the 2D symmetric structures

Configuration	a	b	c	d	e	f
(m_0, b)	(3, 3)	(4, 4)	(4, 4)	(4, 4)	(5, 5)	(6, 6)
number of symmetry operations	1	2	4	4	10	12
n_r	1	2	2	4	5	6
Running time of proposed approach: s	0.0259	0.0974	0.1098	0.1118	0.1097	0.1135
symmetry group	C_1	C_s	C_{2v}	C_{2v}	C_{5v}	C_{6v}
Configuration	g	h	i	j	k	
(m_0, b)	(7, 7)	(10, 10)	(11, 50)	(12, 60)	(12, 58)	
number of symmetry operations	14	20	20	24	2	
n_r	7	10	10	12	12	
Running time of proposed approach: s	0.1070	0.1087	0.1084	0.1138	0.1311	
symmetry group	C_{7v}	C_{10v}	C_{10v}	C_{12v}	C_s	

The results demonstrate that the proposed symmetry detection method is capable of efficient and exact evaluation of the symmetry groups for all the 2D structures. The structure shown in Fig. 3(a) is based on the geometry of an irregular triangle, where the length ratio of three sides is 4: 6: 7. As each node has a different distance r_j to the center (i.e., n_r=1), the structure is effectively recognized as an asymmetric structure. Clearly, this structure has only the identity operation as a symmetry operation, and thus belongs to group C_1. The structure shown in Fig. 3(b) is a kite. Since it has a single symmetry plane along the vertical direction, this structure is detected to be C_s symmetric. Both of the structures shown in Fig. 3(c) and Fig. 3(d) have two symmetry planes, and thus belong to group C_{2v}. The symmetric structures shown in Fig. 3(e-j) are based on the geometries of n-regular polygons (here n=n_r); these structures have n rotations and n reflections, and thus belong to group C_{nv}. Notably, the symmetric structure shown in Fig. 3(k) is designed by removing two members from the structure in Fig. 3(j), which are shown by the thick dotted lines. As a result, the structure has only the identity and a single reflection operation with respect to the thin dotted line as symmetry operations. Therefore, such a structure belongs to the group C_s.

4.2. 3D truss structures

Figure 4 shows a 3D truss structure, which consists of twelve pin-joints and twenty truss members. The height of the structure (along the Z-axis), the length of the outer members, and the length of the diagonal members are h=2m, $l_o = 4$ m, and $l_d = \sqrt{6}$ m, respectively.

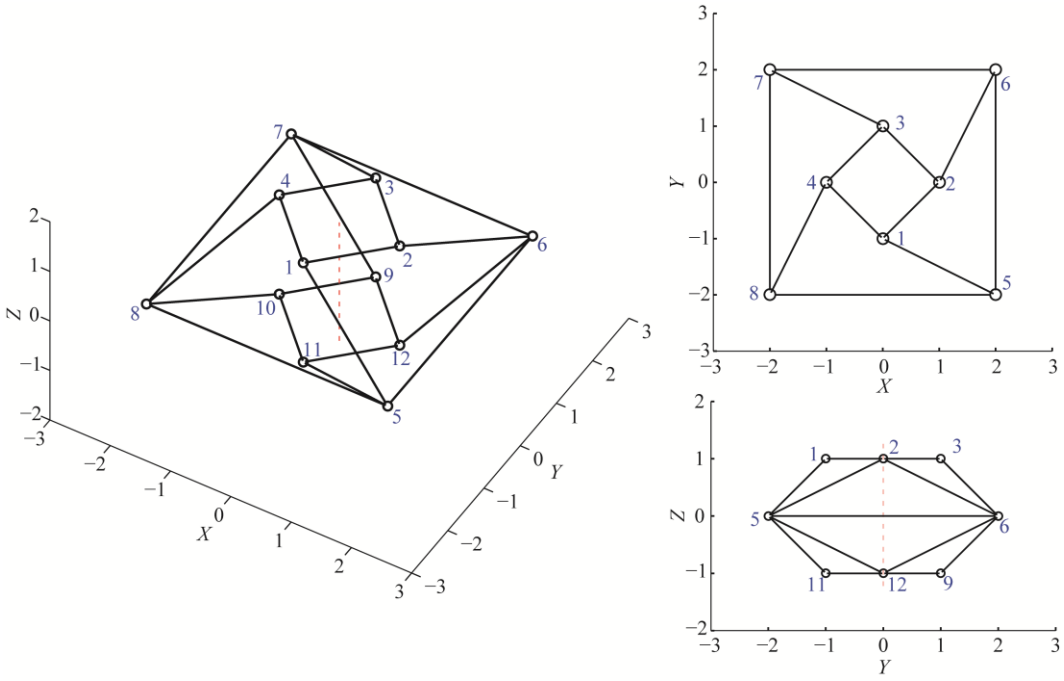

Figure 4 A 3D truss structure

Note that recognizing all symmetry operations for this structure needs only 0.152s. It turns out that $n_r = 8$, because the distances from the nodes 1-4, 9-12 to the symmetry center are identical. Then, the value of *n* for the *n*-fold rotation axis is predicted from Eq. (18)

$$2 \le n \le 8 \tag{29}$$

As expected, it turns out that $n = 4$ and the structure belongs to symmetry group C_{4h}. It remains unchanged under the identity, three rotation operations and one reflection operation σ_h with respect to the horizontal symmetry plane *XY*. Importantly, although the nodes are indistinguishable under four reflection operations σ_v with respect to the vertical symmetry planes ($\alpha_r = 0, \pi/4, \pi/2,$ and $3\pi/4$, respectively), the truss members cannot retain these reflection operations.

Note that the proposed algorithm not only detects the symmetry group for a given structure, but also records the transformations of its nodes and members under different symmetry operations. For example, Table 3 gives the nodal transformations of this C_{4h} symmetric structure, where the first row lists the reference numbers of the nodes of the original configuration.

Table 3 Nodal transformations of the C_{4h} (C_4) symmetric structure under different types of symmetry operations

Symmetry operation	Numbering of nodes											
	1	**2**	**3**	**4**	**5**	**6**	**7**	**8**	9	10	11	12
identity E	**1**	**2**	**3**	**4**	**5**	**6**	**7**	**8**	9	10	11	12
rotation operation C_4^1	**2**	**3**	**4**	**1**	**6**	**7**	**8**	**5**	10	11	12	9
reflection operation σ_h	11	12	9	10	5	6	7	8	3	4	1	2

Obviously, all the nodes remain invariant under the identity E, as the numbering of the nodes remains unchanged. Contrarily, all the nodes move to other positions under the rotation operation C_4^1. For instance, the first two entries in the third row indicate that the shifted nodes 1 and 2 move to coincide with the original nodes 2 and 3 under the rotation. In addition, nodes 5-9 remain invariant under the reflection operation σ_h, while nodes 1, 2, 3, and 4 are respectively transformed from nodes 11, 12, 9 and 10.

In order to check the accuracy and robustness of the automated symmetry detection method, two similar truss structures with different symmetries are presented in Fig. 5. These two structures are based on the configuration of the original structure shown in Fig. 4. The structure in Fig. 5(a) is obtained by removing nodes 9-12 and their adjacent members; the structure in Fig. 5(b) is obtained by modifying nodal coordinates of nodes 1, 3, 10 and 12 (along the Z-axis) from $z = \pm 1\,\text{m}$ to $z = \pm 1.5\,\text{m}$.

The value of n_r reduces to $n_r = 4$ for these two structures. It takes 0.149s and 0.151s, respectively, to complete symmetry detection for the two structures. In comparison to the original structure in Fig. 4, the structure in Fig. 5(a) does not remain unchanged under the reflection operation, and therefore belongs to group C_4. The structure shown in Fig. 5(b) has an identity and a two-fold rotation operation C_2^1, as well as two improper rotations S_4^1 and S_4^3. As a result, this structure belongs to the improper cyclic group S_4.

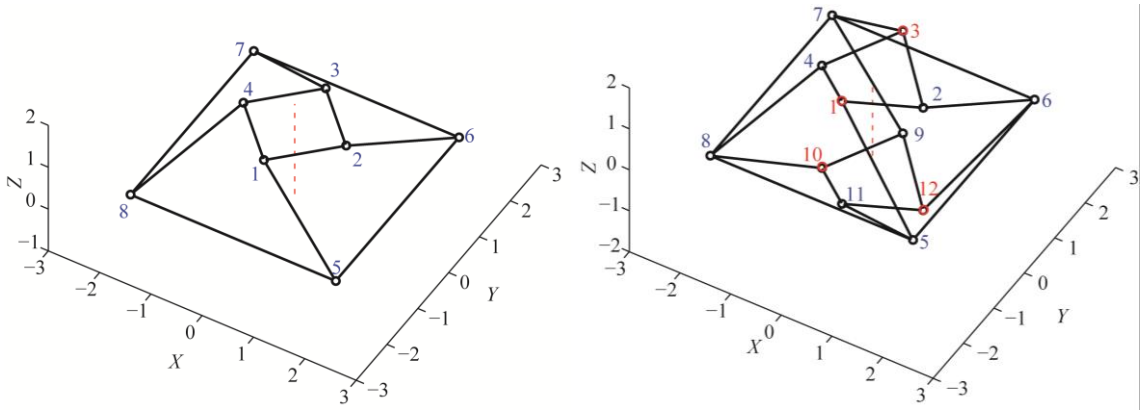

Figure 5 Two different 3D truss structures originated from the structure shown in Fig. 4

The bold entries in Table 3 describe the nodal transformations of the C_4 symmetric structure, and the entries in Table 4 describe the nodal transformations of the S_4 symmetric structure. It can be noticed that all the nodes change their positions under all independent symmetry operations, except the identity operation E.

Table 4 Nodal transformations of the S_4 symmetric structure under different types of symmetry operations

Symmetry operation	Numbering of the nodes											
	1	2	3	4	5	6	7	8	9	10	11	12
identity E	1	2	3	4	5	6	7	8	9	10	11	12
rotation operation C_2^1	2	3	4	1	6	7	8	5	10	11	12	9
improper rotation S_4^1	10	11	12	9	8	5	6	7	2	3	4	1

4.3. A 3D cable-strut structure

A large-scale cable-strut structure is given in Fig. 6. It has a diameter of 120 m and consists of 80 pin-joints and 208 members, with 32 strut members denoted by thick lines and 176 cable members denoted by thin lines. In fact, its geometric configuration is based on the prestressable structure reported in [7], where the two pin-joints along the principal axis and their adjacent members have been removed. The outmost 16 nodes are constrained in the X, Y, and Z directions.

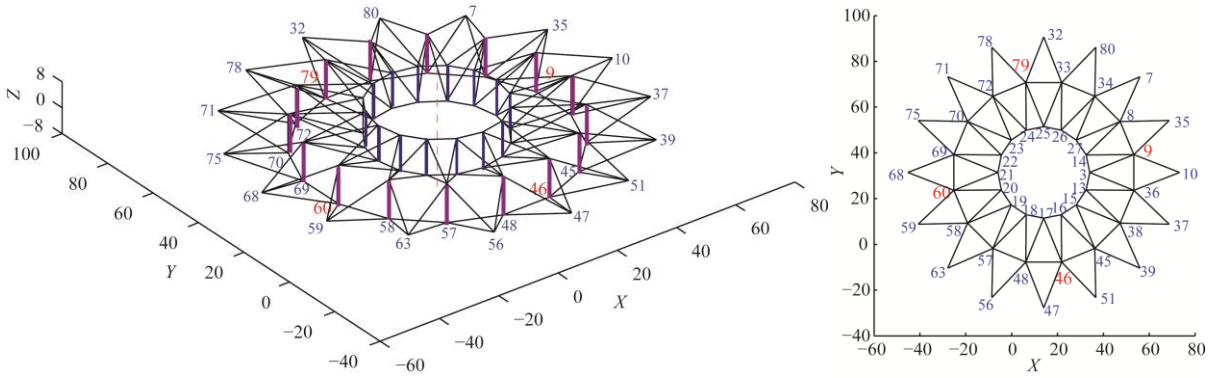

Figure 6 A 3D cable-strut structure with 80 nodes and 208 members

Though the symmetry center is not located at the origin of the coordinate system (Fig. 6), the symmetry detection algorithm effectively detects the symmetry group of this structure. The complete iteration process takes only 0.117s for this highly symmetric structure, which consists of a large number of nodes and members. The value of n_r is computed to be n_r=16. As the structure remains invariant under both 16-fold rotations and reflection operations with respect to the vertical symmetry plane, it is C_{16v} symmetric.

Figure 7 illustrates the nodal transformations of the cable-strut structure under different symmetry operations. Each shifted node is associated with a different position of the original nodes.

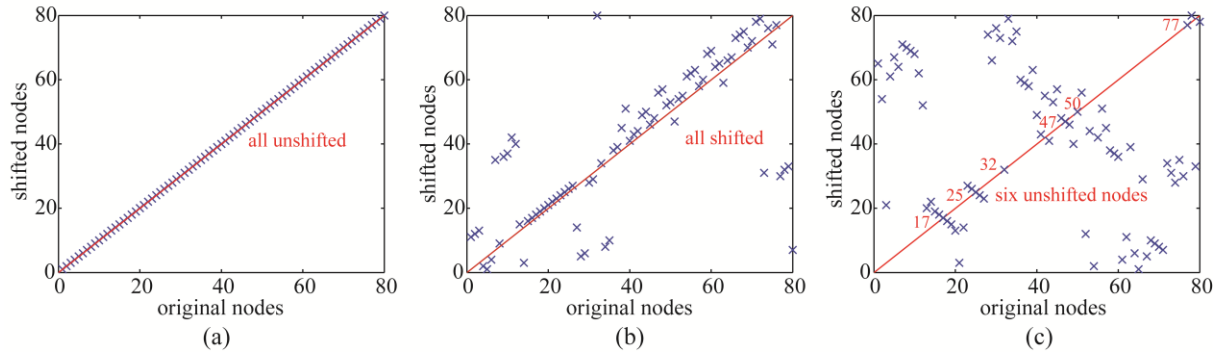

Figure 7 Transformations of the nodes of the cable-strut structure under different types of symmetry operations: (a) identity E; (b) rotation operation C_{16}^{1}; (c) reflection operation with respect to the symmetry plane YZ, with

$$\alpha_r = \pi/2$$

As expected, all nodes are unshifted by the identity operation E (Fig. 7a), and they are shifted by rotation operations (Fig. 7b). Interestingly, six nodes (17, 25, 32, 47, 50, and 77) remains invariant under the reflection

operation with $\alpha_r = \pi/2$, as shown in Fig. 7(c). These unshifted nodes are located on the symmetry plane *YZ*, and are therefore not affected by the symmetry operation.

Recall that the change of boundary conditions, material properties, or cross-sectional areas of members would alter the symmetry of a given structure. For example, if the vertical strut connected to node 9 has a different cross-sectional area from those of the struts on the same orbit [1], its symmetry group is $G_a = C_s$. Then, the symmetry group *G* for the structure is evaluated from Eq. (23),

$$G = \text{lowest-order group of } (C_{16v}, C_s) = C_s \tag{30}$$

In other words, because of the change of cross-sectional area for a member, the highly symmetric structure reduces to be symmetric with a low-order. Similarly, if the struts connected to nodes 9 and 60 (or nodes 9, 46, 60 and 79 in Fig. 6) have a different cross-sectional area, then the structure is C_{2v} (or C_{4v}) symmetric.

4.4. 3D dome structures with different cyclic symmetries

To further validate the feasibility of the proposed symmetry detection algorithm, dome structures with a large number of nodes and members are studied. Such type of dome structures is based on the graph products of a cycle graph with *n* vertices and an arc graph with n_p vertices [41-43]. The diameter of the cycle graph is *L*; the arc graph with n_p vertices denotes a parabola on the vertical symmetry plane, whereas the curve is given by $z = -0.5x^2 + 0.125L^2$ ($0.05L \le x \le 0.5L$). For example, Fig. 8 shows a 3D dome structure with n=18 and n_p=6, which consists of 108 nodes and 378 members.

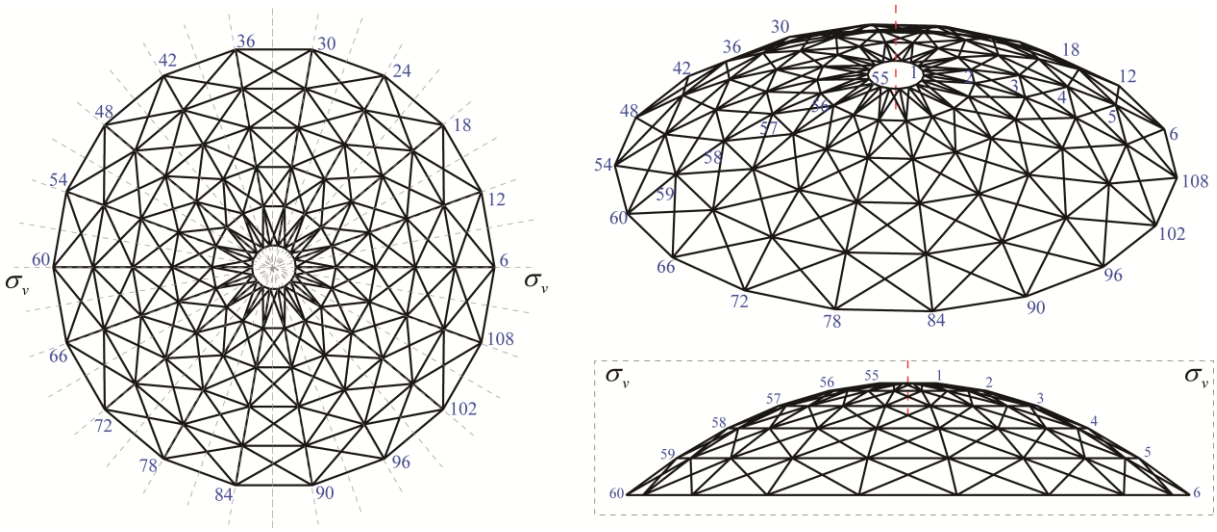

Figure 8 A 3D dome structure composed of 108 nodes and 378 members

As far as the structure in Fig .8 is concerned, a total of 36 independent symmetry operations are recognized by running the proposed algorithm within 0.245s. The symmetry operations include the identity operation *E*, 17 rotation operations, and 18 reflection operations. Thus, this dome structure is C_{18v} symmetric. In addition, distribution patterns for the nodal transformations of this structure under six typical symmetry operations are given in Fig. 9.

These nodal transformations shown in Fig. 9 describe strong regularity. All the nodes are located at the original positions and remain unmoved under the identity operation *E*, while none of the nodes remains unmoved under the proper rotations. Interestingly, twelve nodes remain unmoved under one type of reflection operations (e.g., Fig. 9d and Fig. 9f), while no node stays fixed under the other type of reflection operations (e.g., Fig. 9c and Fig. 9e). This is owing to the fact that twelve nodes are located on the vertical symmetry plane in the former case, and no node is located on the symmetry plane in the latter case.

Furthermore, the impact of structural configurations induced by different values for *n* and n_p is investigated in this study, where the diameter of the cycle graph and the curve of the arc graph remain unchanged. The corresponding contour plots for the number of members and the running time for the structures with variable *n* and n_p are shown in Fig. 10(a) and Fig. 10(b), respectively.

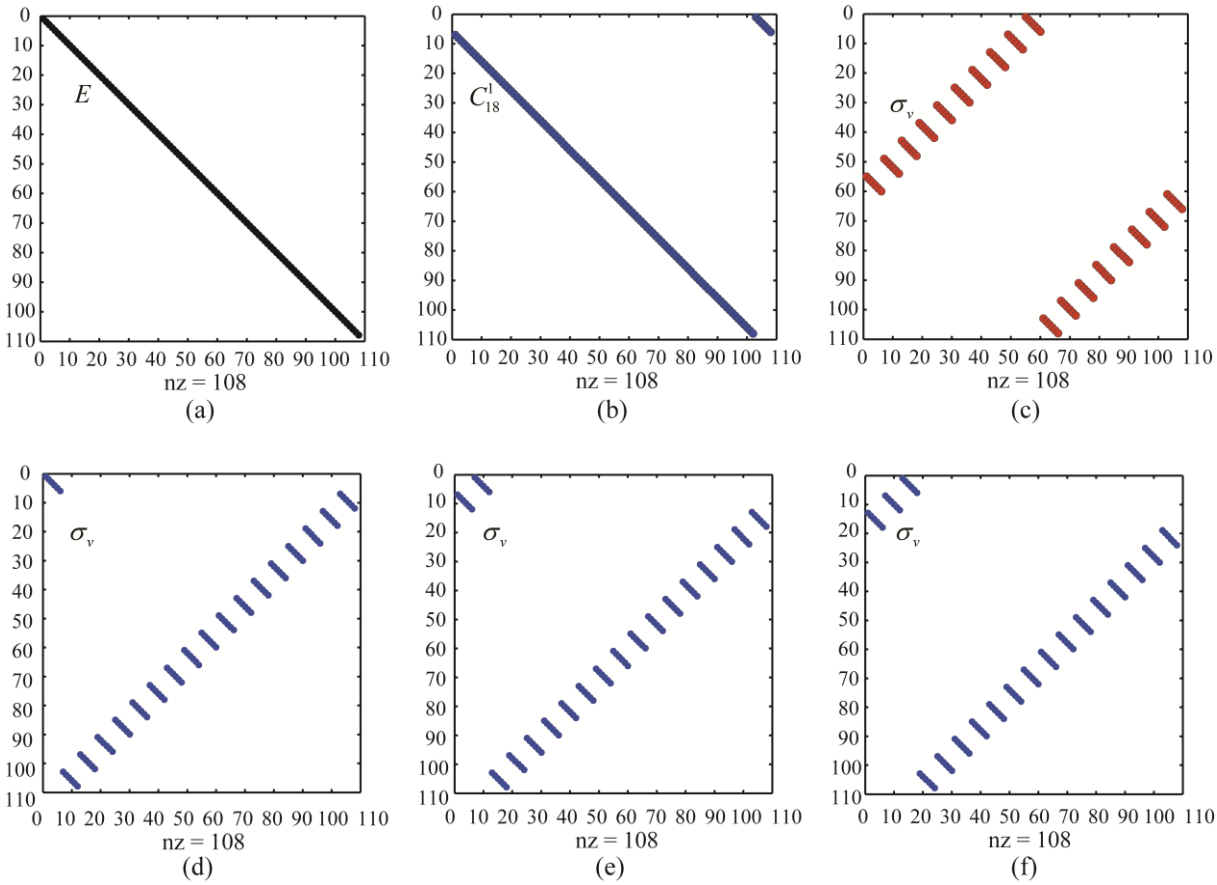

Figure 9 Distribution patterns for nodal transformations of the C_{18v} symmetric dome structure under typical symmetry operations: (a) identity *E*; (b) rotation C_{18}^1; (c) reflection σ_v with $\alpha_r = \pi/2$; (d) reflection σ_v with $\alpha_r = 0$; (e) reflection σ_v with $\alpha_r = \pi/18$; (f) reflection σ_v with $\alpha_r = \pi/9$

It can be noticed from Fig. 10 that both the number of members and the computational effort involved in running this method show nonlinear and significant rise with the increases of *n* and n_p. It turns out that the total number of members can be calculated as $4n \cdot n_p - 3n$, while the structural symmetry remains to be C_{nv} symmetry. It means that this type of symmetric domes has at least $n_r = n$ identical distances from the nodes to the symmetry center, regardless of the variations of *n* and n_p. More importantly, the whole running time for recognizing the structure with the largest number of members is still less than 0.8s (Fig. 10b). Therefore, the automated symmetry detection algorithm is computationally efficient.

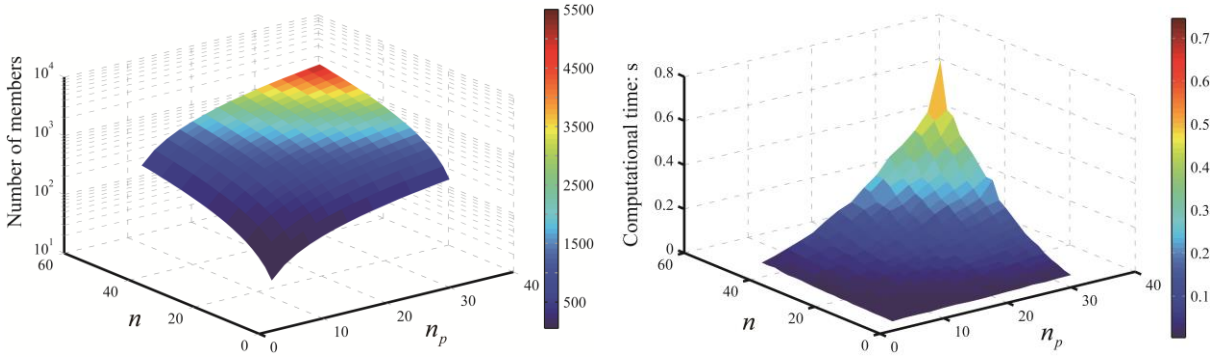

(a) (b)

Figure 10 Contour plots for (a) number of members; and (b) running time for each detection process of the dome structures with variable n and n_p

5. Conclusions

On the basis of five types of symmetry operations and their matrix representations, this study has proposed a computationally efficient method for the automated detection of engineering structures with cyclic symmetries. Only nodal coordinates and connectivity patterns of members are needed in advance. The proposed method offers significant benefit for symmetry detection, such as reducing computational effort, avoiding human errors and enhancing computational accuracy.

To evaluate the feasibility and robustness of the presented symmetry detection method, a great number of 2D and 3D symmetric structures have been studied. The results verify that the automated detection algorithm is accurate and efficient for not only conventional symmetric structures, but also for low-order/high-order symmetric structures with many nodes and numbers. A highly demonstrative example of the method is the exact detection on the C_{18v} symmetric dome structure with 108 nodes and 378 members, which takes only 0.245s. Moreover, the proposed detection algorithm can record the transformations of nodes and members under symmetry operations. This is very helpful to understand the symmetry properties of a structure, and can be utilized for further symmetry analysis.

Acknowledgements

Work supported by the Natural Science Foundation of Jiangsu Province (Grant No. BK20150602), the National Natural Science Foundation of China (Grant No. 51508089 and No. 51578133), the Open Research Fund Program of Jiangsu Key Laboratory of Engineering Mechanics, Southeast University (Grant No. LEM16B10), and the Priority Academic Program Development of Jiangsu Higher Education Institutions. The anonymous reviewers are thanked for their valuable suggestions.

References

[1] Ceulemans A, Fowler PW. Extension of Euler's theorem to symmetry properties of polyhedra. Nature. 1991; 353: 52-4.

[2] Kaveh A, Dadfar B. Eigensolution for Stability Analysis of Planar Frames by Graph Symmetry. Computer-Aided Civil and Infrastructure Engineering. 2007; 22: 367-75.

[3] Ding X, Yang Y, Dai JS. Design and kinematic analysis of a novel prism deployable mechanism. Mechanism and Machine Theory. 2013; 63: 35-49.

[4] Mitschke H, Schroeder-Turk GE, Mecke K, Fowler PW, Guest SD. Symmetry detection of auxetic behaviour in 2D frameworks. EPL (Europhysics Letters). 2013; 102: 66005.

[5] Chen Y, Feng J. Efficient method for Moore-Penrose inverse problems involving symmetric structures based on group theory. Journal of Computing in Civil Engineering. 2014; 28: 182-90.

[6] Wei GW, Chen Y, Dai JS. Synthesis, mobility and multifurcation of deployable polyhedral mechanisms with radially reciprocating motion. Journal of Mechanical Design-Transactions of the ASME. 2014; 136: 91003.

[7] Chen Y, Feng J, Ma R, Zhang Y. Efficient symmetry method for calculating integral prestress modes of statically indeterminate cable-strut structures. Journal of Structural Engineering. 2015; 141: 04014240.

[8] Zingoni A. Group-theoretic exploitations of symmetry in computational solid and structural mechanics. International Journal for Numerical Methods in Engineering. 2009; 79: 253-89.

[9] Guest SD, Fowler PW. Symmetry conditions and finite mechanisms. Journal of Mechanics of Materials and Structures. 2007; 2: 293-301.

[10] Chen Y, Sareh P, Feng J. Effective insights into the geometric stability of symmetric skeletal structures under symmetric variations. International Journal of Solids and Structures. 2015; 69-70: 277-90.

[11] Sareh P, Guest SD. Designing symmetric derivatives of the Miura-ori. Advances in Architectural Geometry 2014: Springer; 2015.p.233-41.

[12] Sareh P, Guest SD. Design of isomorphic symmetric descendants of the Miura-ori. Smart Materials and Structures. 2015; 24: 85001.

[13] Sareh P. Symmetric descendants of the Miura-ori, Engineering Department, University of Cambridge, UK; 2014.

[14] Zingoni A. Group-theoretic insights on the vibration of symmetric structures in engineering. Philosophical Transactions of the Royal Society A: Mathematical, Physical and Engineering Sciences. 2014; 372: 20120037.

[15] Chen Y, Feng J. Generalized eigenvalue analysis of symmetric prestressed structures using group theory.

Journal of Computing in Civil Engineering. 2012; 26: 488-97.

[16] Jiang X, Sun J, Guibas L. A Fourier-theoretic approach for inferring symmetries. Computational Geometry. 2014; 47: 164-74.

[17] Lebmeir P, Richter-Gebert J. Rotations, translations and symmetry detection for complexified curves. Computer Aided Geometric Design. 2008; 25: 707-19.

[18] Lozano-Galant JA, Nogal M, Castillo E, Turmo J. Application of Observability Techniques to Structural System Identification. Computer-Aided Civil and Infrastructure Engineering. 2013; 28: 434-50.

[19] Yeum CM, Dyke SJ. Vision-Based Automated Crack Detection for Bridge Inspection. Computer-Aided Civil and Infrastructure Engineering. 2015; 30: 759-70.

[20] Lee S, Liu Y. Skewed rotation symmetry group detection. IEEE Transactions on Pattern Analysis and Machine Intelligence. 2010; 32: 1659-72.

[21] Loy G, Eklundh J. Detecting symmetry and symmetric constellations of features. Computer Vision-ECCV 2006: Springer; 2006. 508-21.

[22] Zingoni A. Symmetry recognition in group-theoretic computational schemes for complex structural systems. Computers and Structures. 2012; 94-95: 34-44.

[23] Suresh K, Sirpotdar A. Automated symmetry exploitation in engineering analysis. Engineering with Computers. 2006; 21: 304-11.

[24] Highnam PT. Optimal algorithms for finding the symmetries of a planar point set. Information Processing Letters. 1986; 22: 219-22.

[25] Tate SJ, Jared GEM. Recognising symmetry in solid models. Computer-Aided Design. 2003; 35: 673-92.

[26] Lee S, Liu Y. Curved glide-reflection symmetry detection. IEEE Transactions on Pattern Analysis and Machine Intelligence. 2012; 34: 266-78.

[27] Nagaraj BP, Pandiyan R, Ghosal A. A constraint Jacobian based approach for static analysis of pantograph masts. Computers and Structures. 2010; 88: 95-104.

[28] Tran HC, Lee J. Advanced form-finding of tensegrity structures. Computers and Structures. 2010; 88: 237-46.

[29] Zhang JY, Guest SD, Connelly R, Ohsaki M. Dihedral 'star' tensegrity structures. International Journal of Solids and Structures. 2010; 47: 1-9.

[30] Zhang JY, Guest SD, Ohsaki M. Symmetric prismatic tensegrity structures. Part II: Symmetry-adapted formulations. International Journal of Solids and Structures. 2009; 46: 15-30.

[31] Xu Y, Fang G, Lv N, Chen S, Zou JJ. Computer vision technology for seam tracking in robotic GTAW and GMAW. Robotics and Computer-Integrated Manufacturing. 2015; 32: 25-36.

[32] Erol A, Bebis G, Nicolescu M, Boyle RD, Twombly X. Vision-based hand pose estimation: A review. Computer Vision and Image Understanding. 2007; 108: 52-73.

[33] Wu LJ, Casciati F, Casciati S. Dynamic testing of a laboratory model via vision-based sensing. Engineering Structures. 2014; 60: 113-25.

[34] Kettle SF. Symmetry and structure: readable group theory for chemists. Chichester, England: John Wiley and Sons Ltd; 2008.

[35] Zhang JY, Ohsaki M. Self-equilibrium and stability of regular truncated tetrahedral tensegrity structures. Journal of the Mechanics and Physics of Solids. 2012; 60: 1757-70.

[36] Koohestani K. On the decomposition of generalized eigenproblems for the free vibration analysis of cyclically symmetric finite element models. International Journal for Numerical Methods in Engineering. 2010; 82: 359-78.

[37] Ikeda K, Murota K, Yanagimoto A, Noguchi H. Improvement of the scaled corrector method for bifurcation analysis using symmetry-exploiting block-diagonalization. Computer Methods in Applied Mechanics and

Engineering. 2007; 196: 1648-61.

[38] Altmann SL, Herzig P. Point-Group Theory Tables. Oxford, UK: Clarendon Press; 1994.

[39] Kangwai RD, Guest SD, Pellegrino S. An introduction to the analysis of symmetric structures. Computers and Structures. 1999; 71: 671-88.

[40] Harth P, Michelberger P. Determination of loads in quasi-symmetric structure with symmetry components. Engineering Structures. 2016; 123: 395-407.

[41] Kaveh A, Koohestani K. Graph products for configuration processing of space structures. Computers & Structures. 2008; 86: 1219-31.

[42] Chen Y, Feng J. Improved symmetry method for the mobility of regular structures using graph products. Journal of Structural Engineering. 2016; 142: 04016051.

[43] Koohestani K. Exploitation of symmetry in graphs with applications to finite and boundary elements analysis. International Journal for Numerical Methods in Engineering. 2012; 90: 152-76.